Development of a New, Wireless Acquisition System for EMATs Compatible With the Robotics Operating System

Arnau Garriga-Casanovas, Pouyan Khalili, and Frederic Cegla, *Member, IEEE*

***Abstract*—The deployment of transducers to perform *in situ* inspections of industrial components can be complicated, and in many cases is still performed manually by a team of operators, which involves significant costs and can be dangerous. Robots capable of deploying probes in difficult to access locations are becoming available. Electromagnetic acoustic transducers (EMAT) are well suited to be used with robots since they are non-contact transducers that do not require a coupling medium, and can easily perform scans. However, existing acquisition systems for EMATs are generally not suitable to be directly mounted on robots. In this paper, a new wireless acquisition system for EMATs is presented. The system is standalone, it transmits the inspection data over WiFi, and is compatible with the robotics operating system (ROS). In addition, it is designed to be modular, small and lightweight so that it can be easily mounted on robots. The system design in terms of hardware and software is described in this paper. The resulting performance of the system is also reported.**

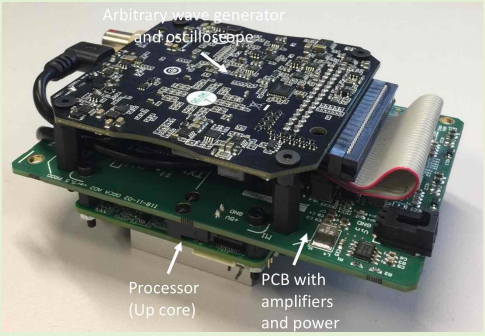

***Index Terms*— Electromagnetic acoustic transducer, non-destructive evaluation, wireless, acquisition system, robotics.**

I. Introduction

AN IMPORTANT part of industrial components suffer from material degradation over their lifetimes. This is particularly relevant in the offshore industry, where exposure to a harsh environment and to corrosive chemical products, such as oil extracted from the ground and additives, significantly accelerates material degradation. Regular inspections are thus generally necessary to ensure safety, and to reduce the maintenance cost. In the offshore industry, these inspections are often performed *in situ* since the cost of dismantling components to inspect them off-site is relatively high.

Currently, a large fraction of the *in situ* inspections of industrial components are performed manually (or in a semi-automated way) by an operator that needs to deploy a probe in the location of interest. The probe is then often scanned over the surface to gain more information. This operation can be complicated, either due to difficult access to the component of interest, or due to the hazardous environment where the component is located. These complications significantly increase the cost of the inspection, as they can require the building of scaffolding or the need for ropes to enable the operator to reach the desired location. Furthermore, sometimes safe access cannot be guaranteed without an outage which can result in the large financial burdens due to loss of production. This increase in costs is particularly relevant in offshore environments such as oil and gas platforms, where the cost of access for the inspection can represent 75% or more of the total inspection cost.

Robotic platforms capable of reaching difficult to access locations and operating in harsh environments are becoming available. Examples of these platforms are unmanned aerial vehicles [1], robotic arms mounted on a mobile robotic base [2], [3], legged robots capable of locomotion on uneven surfaces [4], [5], and underwater vehicles [6], [7]. In addition, there are on-going efforts to further develop these robots for inspections. One example of these efforts is the Offshore Robotics for the Certification of Assets (ORCA) hub [8], which is a combination of industrial companies and academic institutions that supported this work. Another example of these efforts is the SPRINT ROBOTICS initiative [9], which brings together industrial companies to accelerate the advancement of robots for maintenance. These new robotic platforms being developed for inspections require probes and inspection

Manuscript received April 19, 2020; revised June 4, 2020; accepted June 8, 2020. Date of publication June 15, 2020; date of current version October 2, 2020. This work was supported by EPSRC under Grant EP/R026173/1. The associate editor coordinating the review of this article and approving it for publication was Prof. Aime Lay-Ekuakille. *(Corresponding author: Arnau Garriga-Casanovas.)*

The authors are with the Non-Destructive Evaluation Group, Imperial College London, London SW7 2AZ, U.K. (e-mail: a.garriga-casanovas14@imperial.ac.uk).

Digital Object Identifier 10.1109/JSEN.2020.3002418

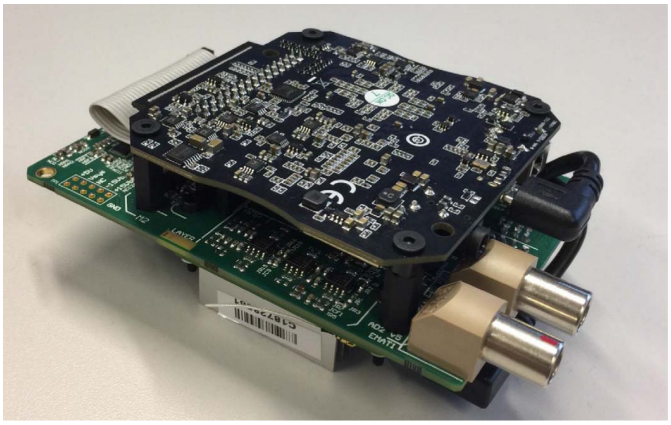

Fig. 1. Acquisition system without enclosure. The system in the image includes a processor, a PCB with amplifiers and power regulation, and an arbitrary wave generator and oscilloscope.

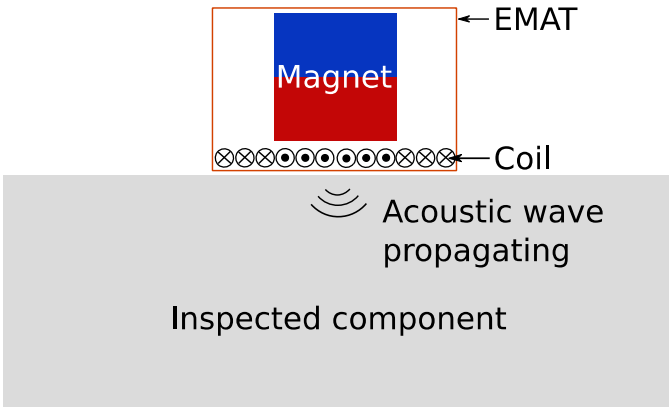

Fig. 2. Schematic diagram of an EMAT probe.

equipment compatible with them, so that the combination of the new robots and equipment can address the inspection needs of industry.

Electromagnetic acoustic transducers (EMATs) are a type of transducer that employ electromagnetic induction to generate and receive ultrasonic waves on components [10], [11]. EMATs generally consist of two main components: a coil and a magnet, as schematized in Figure 2. The coil is typically excited with a current pulse and induces eddy currents on any conductive component placed near it. These eddy currents interact with the magnetic field from the magnet, and generate a Lorentz force, which creates a strain in the material. This strain propagates as an acoustic wave, and reflects on the internal features of the component. The reflected waves are received by the same EMAT through an equivalent mechanism and can be processed to obtain inspection information.

In general, EMATs can be used for thickness measurement, by analyzing the time of flight of the wave, or for crack detection, by analyzing the amplitude of the waves received [11], [12]. The use of electromagnetic induction in EMATs implies that they can be used to perform non-contact inspections, inspections of components with thin coatings, and inspections of components with significant surface roughness, for example due to corrosion. Furthermore, EMATs can be easily used to scan components without the need for a coupling medium. As a result, they are well suited for use with robots.

The generation of the current pulse for EMATs, and the reading of the received electrical signals from it needs to be performed using an acquisition system. Existing acquisition systems for EMATs tend to be relatively voluminous and heavy, they generally employ high power electronics that cannot be used in explosive environments, and in many cases they use software that can be difficult to interface with a robot. As a result, they cannot be easily mounted on typical robotic platforms. In this regard, there is a need for an acquisition system that is relatively small, lightweight, low power, easy to integrate and compatible with standard robotics software, such as the robotics operating system (ROS) [13].

In this paper, a new acquisition system for EMATs is presented, which is developed to be suitable for robotic inspections. The new system, shown in Figure 1, is relatively small, lightweight, modular, ROS-enabled, uses low power electronics, and is wireless as it transmits the acquired data over Wi-Fi communication. In addition, the system is versatile since it can be directly used with an EMAT probe.

The performance of the acquisition system developed in this work is also reported. The performance is evaluated in four different configurations in terms of inspection scenario and method. This also serves to showcase the versatility of the acquisition system, which can perform all the different inspections.

The rest of the paper is structured as follows. The design of the acquisition system in terms of both hardware and software is described in Section II. The methods used to experimentally test the performance of the system are reported in Section III. The results of the experimental tests are presented in Section IV, together with a discussion of the performance of the acquisition system. Lastly, concluding remarks are summarized in section V.

II. Acquisition System Design

The design of the acquisition system is presented in this section. The requirements for the acquisition system are summarized in subsection II-A. The hardware design of this acquisition system is presented in subsection II-B, and the software design in subsection II-C. The complete acquisition system with the typical elements for operation is presented in subsection II-D.

A. Requirements

The acquisition system needs to be a self-contained system capable of generating and reading the electric signals required to acquire data from practically any EMAT probe. The electrical signal for excitation of an EMAT probe is typically a voltage pulse that can be in the order of 30 V, and consists of a five-cycle tone-burst with a wave frequency that can range between 100 kHz to 5 MHz. The received electrical signals from the EMAT are typically in the order of millivolts, and consist of an analogue time-trace of measured voltage. This time-trace needs to be amplified and recorded without adding significant noise.

The acquisition system also needs to be capable of processing the acquired signals, so it requires some computing

capability. Lastly, the acquisition system also should be capable of transmitting the data of interest over Wi-Fi using ROS.

An acquisition system with a single channel can be used for thickness measurement. However, a system with two channels is required for crack detection. This is due to the fact that EMAT probes for crack detection have two independent coils that excite waves polarized in perpendicular directions in the material [14]. These two waves polarized in perpendicular directions interact differently with any potential crack, with one of the two waves being significantly more attenuated that the other due to the crack. The ratio of amplitudes between the two waves can thus be used to infer the presence of a crack. In this regard, two independent channels are desired in the acquisition system.

B. Hardware

Considering these requirements, the hardware of the acquisition system developed in this work consists of three main elements. The first is an arbitrary function generator to generate, and an oscilloscope to read, the electric signals. The oscilloscope proposed in this work has two channels to acquire data simultaneously from two coils on any EMAT probe. The generator can produce arbitrary shaped waveforms with frequency content between 100 kHz and 5 MHz. The second element in the system is an analogue amplifier, which amplifies the signals received from the EMAT probe. In this work, this is custom designed to achieve signal amplification of $\sim$70 dB in the received voltages from the EMAT probe. The third element is a machine with processing power and Wi-Fi, which controls the oscilloscope, performs the required processing on the data obtained, and transmits the data of interest over Wi-Fi using ROS. In this work, an Up Core, supplied by Aaeon (Taipei, Taiwan), is selected for this third element. The Up Core is a system on a chip that has a Wi-Fi module embedded on it at the frequency spectrum of 2.4 GHz, and sufficient RAM, computing power and internal memory to run ROS and perform signal processing without delays. The suitable performance of this processor is confirmed in the performance results in section IV. In addition, accessories for the Up Core are available to expand it with Wi-Fi at 5 GHz frequency to add redundancy to the system when required.

The system is wireless, so the power for it is supplied by an on-board battery. In this work, this is a lithium-ion battery that supplies a voltage of 11.1 V and has a capacity of 2.6 Ah. The voltage of the battery needs to be regulated to the different voltages required for the different elements of the system. This is achieved with custom power regulation electronics, which are also incorporated into the system.

The connection and integration of the three main elements of the system, together with the battery and power regulation electronics, is achieved with a custom printed circuit board where all the components are assembled. All the hardware used in the system employs low power electronics, and the maximum power is 15 W. A prototype of the acquisition system, where all the hardware is assembled, is shown in Figure 1, and a block diagram of its main elements is shown in Figure 3.

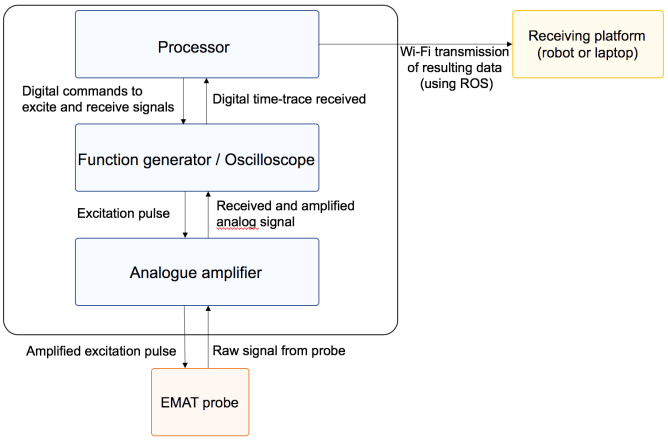

Fig. 3. Block diagram of the complete acquisition system. The main components of it are schematized, as well as the communication between them. The interaction of the system with an EMAT probe (illustrated in orange), and with a receiving platform (illustrated in yellow), are also depicted.

C. Software

The acquisition system is centrally controlled by the Up Core. In this work, the Ubuntu 16.04 operating system is installed on it. This interfaces with the oscilloscope board through a USB connection. The data acquired from the oscilloscope is also processed on the Up Core to extract the information of interest. This information is typically either a thickness value of the inspected component, or the ratio of amplitudes of two coils on the EMAT probe that polarize waves in orthogonal directions, which is indicative of the presence of a crack.

The information of interest is then transmitted over Wi-Fi by the same Up Core to any robot or independent laptop. For this, an *ad hoc* Wi-Fi connection is created by the Up Core, where the robot or independent laptop can connect. This enables the use of the acquisition system in any location, without the need for external internet connection. The connection between the acquisition system and the robot or independent laptop and the Up Core is established using the network protocol secure shell (SSH).

In this work, ROS is installed on the Up Core. The processes on the Up Core to acquire data from the oscilloscope, process it, and transmit it over Wi-Fi, are implemented using ROS nodes on the Up Core. This is performed automatically by executing a single launch file on the robot or independent laptop, which establishes the SSH connection with the Up Core, and executes the required nodes on it.

D. Complete System

The main elements of the complete acquisition system, together with the communication between them, are summarized in a block diagram shown in Figure 3. As previously mentioned in subsection II B, the system consists of three main components, namely the processor, function generator/oscilloscope, and analogue amplifier. The components are arranged vertically in Figure 3, from higher level operations at the top to lower level operations at the bottom. In a typical acquisition, the processor initiates the data acquisition command, which then follows the downward black arrows in

Figure 3 until the EMAT probe is excited. Then the returning raw signals from the EMAT probe follow the upward black arrows, being amplified and digitized and received by the processor. The information of interest is lastly communicated via Wi-Fi to the receiving platform, shown in yellow in Figure 3.

The complete acquisition system can be assembled into an enclosure of size 145 × 85 × 43 mm, shown in Figure 3. The system weighs 140 g excluding the battery, and 310 g including the 2.6 Ah battery and an enclosure box. The battery can also be directly exchanged for a different battery to suit the requirements of duration and weight of each application, provided that the selected battery supplies a voltage between 10 V and 14 V.

The system offers two acquisition channels, so it can be used with both single or dual-coil EMAT probes to perform thickness measurements or detect cracks. The system can also be directly used with other EMAT probes, e.g. to generate guided waves as described in the next section III.

The thickness of components is determined using the echoes from the reflection of the generated wave pulse on the back wall of the component. In particular, the time of arrival of the first and second echo from the back wall is determined by the system from the recorded time-trace. Then, the thickness of the component is calculated as

$$d = \frac{vt}{2} \tag{1}$$

where v is the velocity of the mechanical wave propagating in the material, and t is the time span between the first and the second echo from the back wall. An example of time-trace that contains the first, second, and subsequent echoes from the back wall is shown in the results section in Figure 6.

The use of the acquisition system is straightforward by simply connecting an EMAT probe with a LEMO connector, and interfacing with the system via Wi-Fi using an independent laptop or any robot with ROS. The use of the complete acquisition system with an EMAT probe and a laptop is also shown in Figure 2, and examples of its use are presented in the next section III.

III. Experimental Testing

The resulting acquisition system can be used to acquire data with different EMAT probes, and transmits the data to any robot or laptop with ROS installed on it. In order to evaluate and showcase its performance, the acquisition system was tested in a set of experiments described in this section.

The system was first tested with a single-coil EMAT probe placed on a 10 mm steel plate, and receiving data on a laptop running ROS. This is a typical inspection setup to measure thickness of a plate, and is equivalent to the set up shown in Figure 4 where the probe is placed on a test sample and connected to the acquisition system. The EMAT probe was excited with a 5-cycle tone-burst of a 2 MHz frequency. Ten time-traces were acquired and averaged to produce the resulting inspection signal. The system was then tested with the same single-coil EMAT placed on an 8 mm thick steel plate with a paint coating that is representative of those used in industry to prevent corrosion. The setup

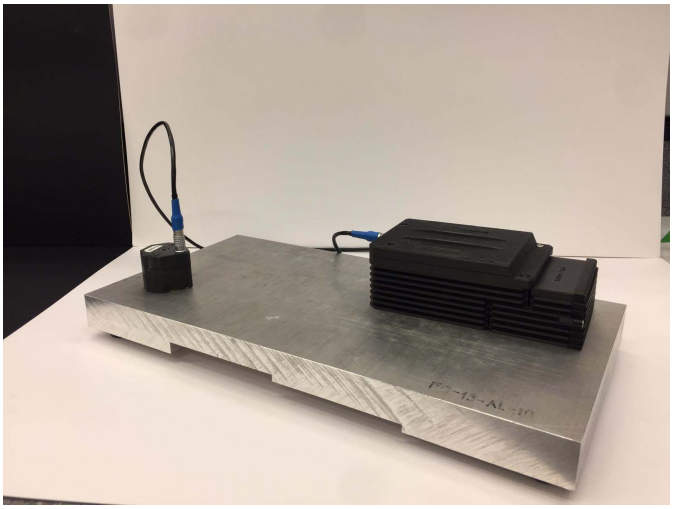

Fig. 4. Typical set up for use of the acquisition system with a standard EMAT probe.

was equivalent and, as in the previous case, ten time-traces were acquired and averaged. Fifty averaged acquisitions in this same configuration were obtained in order to determine the repeatability and accuracy of the system. Lastly, the system was tested with the same single-coil EMAT placed on a 29.5 mm thick aluminum block, since it is a material with different properties, particularly in terms of higher electrical conductivity and the fact that it is non-ferromagnetic. This provides a relevant reference of versatility of the system when used in different materials that are representative of those that can be found in industry. since it is a material that typically presents lower noise levels due to grain scattering, and thus provides a relevant reference to illustrate the source of noise. As in the previous two cases, the setup was equivalent and ten time-traces were acquired and averaged.

The acquisition system was also tested in a second configuration corresponding to a guided wave inspection, in order to showcase the versatility of the system. In that case, the system was connected to a particular EMAT probe that consists of an array of magnets with alternating polarizations arranged with a spacing that matches the desired excitation wavelength. The EMAT also has an excitation coil underneath, as shown in Figure 5. The probe was placed on a 10 mm thick aluminum plate that had a 1 mm deep notch across the entire plate. The notch is perpendicular to the propagation direction of the excited wave, as shown in Figure 5. The distance between the probe and the notch was 250 mm. The acquisition system was used to excite a tone-burst with a wave frequency of 300 kHz, and receive the returning signals. The system was then subsequently tested in an equivalent set up, but placed on a plate without a notch and with a transmitter and an identical receiver EMAT that were separated by a distance of 500 mm. The same excitation tone-burst with a wave frequency of 300 kHz was used. This test in a plate without a notch and using two separate EMATs to transmit and receive signals was conducted as a reference measurement of the signal amplitude. Lastly, the system was tested in the same configuration, but using a single EMAT place on a plate without a notch to show the signals in a case without any reflection from the notch.

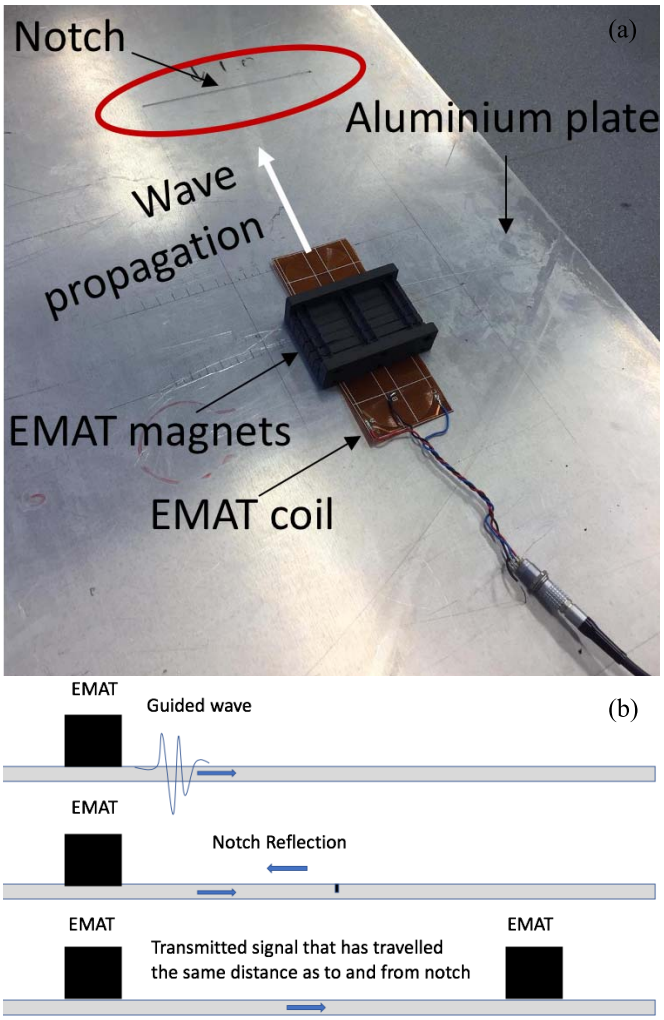

Fig. 5. (a) Set up for testing the acquisition system with a probe to excite guided waves. In the picture, probe is placed on a 10 mm thick aluminum plate with a notch that is 1 mm deep, which is representative of a crack; the direction in which the excited guided wave propagates is indicated with a white arrow. (b) Schematic of the three tests in three different configurations, which correspond to: (top) a guided wave excited with a single EMAT in a plate without defects and without boundaries; (middle) a guided wave excited in a plate with a notch; and (bottom) a guided wave excited with a transmitting EMAT and received with a receiving EMAT separated a certain distance.

Finally, the acquisition system was tested in a configuration corresponding to a scan of a component. In this case, a single-coil EMAT probe was used to measure the component thickness. The probe was initially placed near one end of the component, and was manually scanned over the surface of the component while collecting the inspection data and transmitting it to a receiving laptop. The component used was an aluminum plate with four thickness steps corresponding to 29.5 mm, 25 mm, 20 mm, and 29.5 mm, which is shown in Figure 12. For each inspection measurement, the probe was excited with a 5-cycle tone-burst of a 2 MHz frequency, and time-traces were acquired and averaged. The resulting time-trace signal was then processed by the acquisition system to determine the component thickness. The resulting value was then transmitted via Wi-Fi using ROS to the laptop, also running ROS. The procedure was repeated in a loop during the scan to obtain the thickness measurement points.

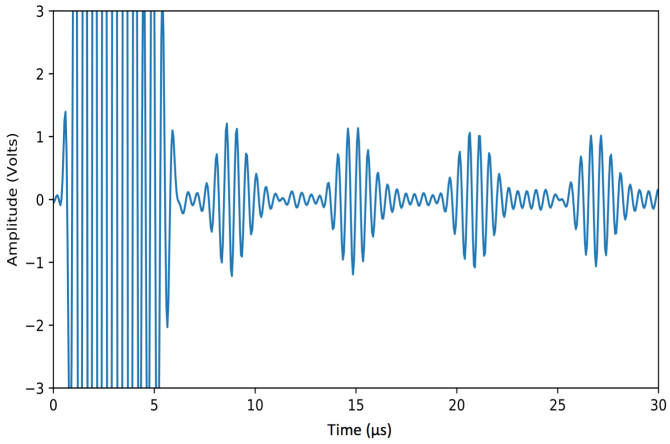

Fig. 6. Time-trace obtained with the acquisition system and an EMAT probe on a 10 mm thick steel plate, with 10 averages.

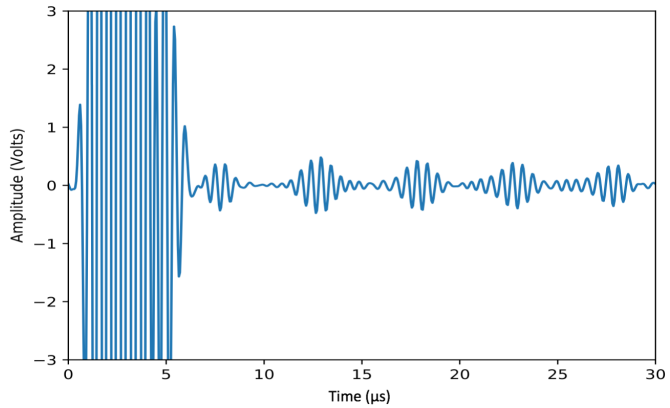

Fig. 7. Time-trace obtained with the acquisition system and an EMAT probe on an 8 mm thick steel plate with paint layer, with 10 averages.

IV. Results and Discussion

The results of the experimental tests to evaluate and showcase the performance of the acquisition system are reported in this section.

The averaged time-trace obtained in the 10 mm steel plate is shown in Figure 6. As can be seen, the resulting signal contains the excitation pulse, the first reflection from the back wall, and the subsequent reverberations from the back wall. The SNR of the resulting signal is 25 dB. This SNR, expressed in dB, is determined according to the following ratio of amplitudes

$$SNR = 20 \log \frac{S_{max}}{N_{max}} \tag{2}$$

where S_{max} is the maximum amplitude in the first echo peak, and N_{max} is the maximum amplitude in the noise between the first and second echoes. The resulting time-trace shown in Figure 6 can be used to determine the plate thickness in a reliable manner, based on the time between the first and second echo, and the use of equation (1).

The averaged time-trace obtained in the 8 mm steel plate with a paint coating is shown in Figure 7. As in the previous case, the resulting signal contains the excitation pulse, the first reflection from the back wall, and the subsequent reverberations from the back wall. The signal amplitude is lower than that shown in Figure 6, which is due to the fact that the coating

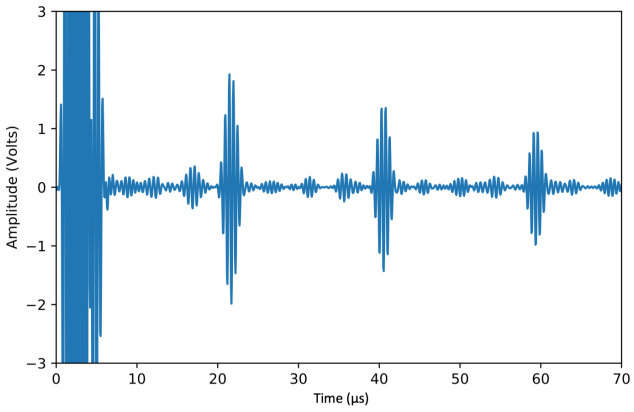

Fig. 8. Time-trace obtained with the acquisition system and an EMAT probe on a 29.5 mm thick aluminum block, with 10 averages.

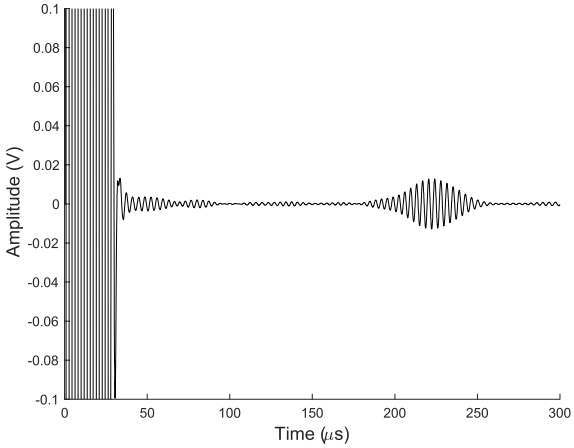

Fig. 9. Time-trace corresponding to a guided wave generated on a 10 mm thick aluminum plate, and reflecting on a 1 mm deep perpendicular notch across the entire plate.

increases the lift-off of the probe, and thereby reduces the intensity of the excited signal. It should also be noted that the test plates used to obtain the results in Figures 6 and 7 are two separate plates. Thus, even though both plates are made of mild steel, the specific material properties are not necessary exactly equal which can also affect the absolute signal amplitude. However, the SNR is equivalent, as the amplitude of the noise is also reduced.

The fifty measurements conducted using the same setup on a 10 mm thick steel plate with 10 averages all led to reliable thickness measurements of the plate of 10 mm $\pm$ 0.08 mm. As in the previous case, the thickness was determined using equation (1). This resulting accuracy of the system is suitable for standard plate inspections.

The averaged time-trace obtained in the 29.5 mm thick aluminum plate is shown in Figure 8. The SNR in this case is approximately 15 dB. The time of arrival of the back wall echoes in the aluminum plate, shown in Figure 8, is approximately 22 μs. This is significantly longer than that in the steel plate, shown in Figure 6, and is due to the fact that the aluminum plate is significantly thicker, and the wave propagation velocity is different from that in steel.

The time-trace in Figure 8 also shows fluctuations in the noise levels between the echoes, which form a set of ripples in the noise. These are attributed to main two sources. One source of the ripples are mode-converted wave reflections, in which the excited shear wave is converted into a longitudinal wave. These mode-converted wave modes have a different propagation speed, since longitudinal waves travel at faster speed than shear waves, and thus have different arrival times than the main back wall echoes from purely shear waves. However, the mode-converted waves also have lower amplitude, and thus they do not mask the signals of interest. Another source of the ripples are internal resonances in the probe and in the electrical elements of the system. Nonetheless, the amplitude of these combined noise fluctuations remains significantly lower than the amplitude of the received signals of interest, which are the back wall echoes, and thus can be clearly differentiated without affecting the inspection reliability.

The time-trace obtained using the acquisition system to generate a guided wave at a frequency of 300 kHz in a plate with a notch (which corresponds to the configuration schematized in Figure 5 (b) (middle)) is shown in Figure 9. The time-trace shows an echo at approximately 225 μs from the excitation. This echo corresponds to the excited guided wave that reflects at the 1 mm deep notch, which can be used for the detection of the crack.

The type of echo shown in Figure 9 occurs when a guided wave propagating on a plate interacts with a surface-breaking crack that is perpendicular to the direction in which the wave propagates. In the test set up shown in Figure 5, the probe excites a guided wave that propagates in the direction shown with a white arrow. This guided wave encounters a 1 mm deep notch perpendicular to it, which is representative of a surface-breaking crack. The incident guided wave partially reflects on the notch or crack (which in the experiment is 10% of the plate thickness), and thus a reflected guided waves propagates back to the excitation probe. The amplitude of the reflected wave is a fraction of the amplitude of the incident wave, and this fraction depends on the depth and width of the crack. In the experimental set up reported in this work, the width of the notch is significantly larger than the spread of the excited wave, and thus acts as an infinitely wide notch. The amplitude of the reflected wave (and therefore the fraction of energy that is reflected) is then determined by the notch depth, which in this case is 1 mm (10% of the plate thickness).

The detection of cracks using guided waves is a subject widely studied in the literature [15]. The method described in this work to excite guided waves using the acquisition system for EMATs presented here is mainly aimed at detecting surface-breaking cracks that are perpendicular to the propagation of the excited guided wave, which corresponds to the test set up presented here. This is illustrative of two typical inspections in industry: (i) the inspection of large plates for large cracks, (ii) the inspection of pipes for cracks in the radial-axial direction. The method for detecting cracks in case (i) is the same as that described in the previous paragraph. The method to detect cracks in (ii) is equivalent, and involves exciting a guided wave using the same probe and acquisition system from one location on the pipe. This guided wave is excited to propagate circumferentially around the pipe. When the wave encounters a crack lying in the radial-axial plane, it reflects from it in an equivalent manner as a wave reflecting

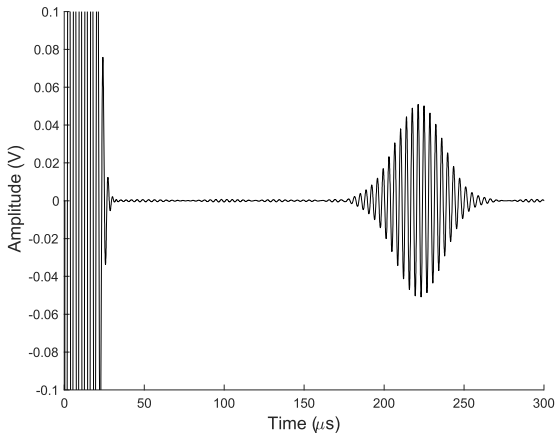

Fig. 10. Time-trace corresponding to a guided wave generated on a 10 mm thick aluminum plate without any defects, and received in a pitch-catch configuration.

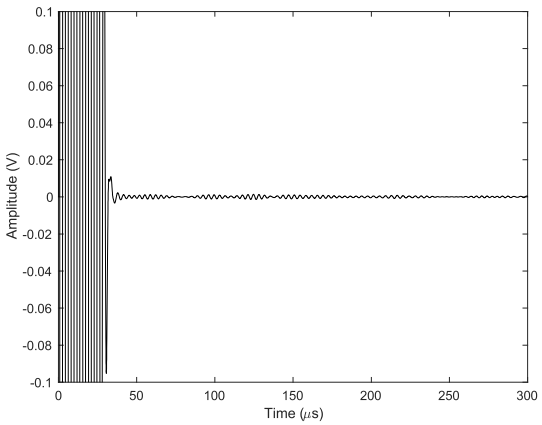

Fig. 11. Time-trace corresponding to a guided wave generated with a single EMAT probe on a 10 mm thick aluminum plate without any defects.

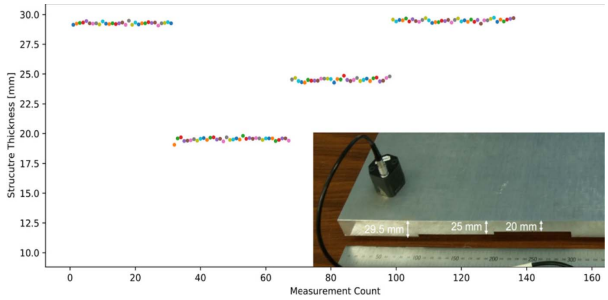

Fig. 12. Resulting thickness values in millimeters received in a laptop using ROS, which are generated by an EMAT scanned over a component with three different thicknesses of 29.5 mm, 24.5 mm, and 20mm. (Inset at bottom right) set up for scanning the aluminum plate with thickness steps.

from a crack in a plate. This reflection then returns to the probe to be received by the acquisition system.

The time-trace obtained using the acquisition system to generate a guided wave on a plate without a notch using a transmitting EMAT, and receive it with a separated receiving EMAT (configuration schematized in Figure 5 (b) (bottom)), is shown in Figure 10. This is presented as a reference test in a case of a wave simply travelling between two EMAT probes in a plate without a notch, where any wave energy losses are only due to wave propagation over the travelled distance. As can be seen in Figure 10, the time of arrival of the wave is equivalent to that in Figure 9. This is intended in the experiment design, and is achieved by placing an excitation probe and a receiving probe at a distance equal to twice the distance between the excitation probe and the notch in the experiment for Figure 9. In this way, the reduction in amplitude due to the travel distance of the wave, or in other words the wave energy loss due to wave propagation, is equal in the experiments corresponding to Figures 9 and 10. The amplitude of the wave in Figure 9, however, is lower than that in Figure 10. This is due to the fact that the wave received in Figure 10 is simply travelling on the plate, and the energy losses in that case are only due to propagation. Instead, the wave received in Figure 9 corresponds to the wave that travels on the plate, is reflected by a 1 mm deep notch and returns to the EMAT in receiving mode. The wave reflected by the notch is only a fraction of the original wave incident on the notch. Thus, the energy of the wave received in Figure 9 is reduced by both the wave propagation, which is the same as the wave in Figure 10, plus the fact that only a fraction of the original wave energy is reflected by the notch. The result is that the echo in Figure 9 is lower than that in Figure 10, and the ratio of amplitudes between Figures 9 and 10 corresponds to the fraction of energy that is reflected by the notch.

Lastly, the time-trace obtained using the acquisition system to generate a guided wave on a plate without any defects and using a single EMAT probe (configuration schematized in Figure 5 (b) (top)), is shown in Figure 11. As can be seen, the time-trace shows no echoes. This is due to the fact that the wave simply travels away from the excitation probe on a plate that is practically infinite without any reflections, and thus no signal returns to the probe.

The results from these experiments also illustrate the versatility of the acquisition system, which can be also used to perform guided waves inspections without any major changes to it.

The result of scanning an EMAT probe over a plate with different thicknesses is shown in Figure 12. Each inspection measurement, which corresponds to a thickness value, is plotted as a dot in Figure 12. As can be seen, the system correctly measures the thickness of the component as the probe is manually moved along its surface. The variation between the thickness measurements at each of the plate steps is within ± 0.1 mm of the average measured thickness value, or in other words, the accuracy of the system is ± 0.1 mm. This is partially due to noise in the system, and partially due to experimental imperfections such as uneven material properties or uneven surface.

This experimental set up comprises thicknesses between 20 mm and 29.5 mm. The system in general is capable of measuring thicknesses within a range approximately between 4 mm and 100 mm when used in components typically found in industry, such as aluminum or steel plates. However, the specific SNR of the inspection, and thus the thickness range that can be inspected reliably, depends on each specific inspection case.

When used to scan components with varying thickness, such as that shown in Figure 12, the system is capable of measuring

any thickness variations that are within the thickness range (typically between 4 mm and 100 mm approximately although depending on the SNR of each specific inspection case), and greater than the system accuracy (±0.1 mm).

Lastly, the main specifications of the acquisition system in terms of practical operation were also characterized during the experiments. The acquisition system offers a range of 20 m in the data transmitted over Wi-Fi to the receiving laptop or robot, when used with a miniature antenna consisting of a 3 cm long wire. Greater range can be obtained using larger antennas. The system can operate for 1.5 hours, continuously measuring and transmitting data, with a 2.6 Ah battery.

The speed of the acquisition system is also suitable for typical inspection requirements. At a frequency of 3 Hz, the system can perform the entire process of obtaining an A-scan with 10 averages, process the data to determine the thickness of the component, and transmit the resulting data continuously and reliably. The SNR of the system is 25 dB on a representative steel plate, and 15 dB on an aluminum plate, as previously reported. The accuracy of the system for thickness measurement is ±0.1 mm when maintaining the EMAT probe in a single location, as previously reported. The received data can be visualized in real time on the receiving robot or laptop, to show the thickness profile of the inspected component, as in the scan test shown in Figure 12. It should be noted that the performance of the system reported in this paper is evaluated in lab tests that aim to be representative of those found in industry, but field tests are required to validate the performance for industrial use.

V. Conclusions

A wireless acquisition system to control EMAT probes was presented in this work. The system is standalone, and is relatively small and lightweight, so it can be easily incorporated into a robotic platform for inspections. The system is ROS-enabled, and transmits the data acquired over Wi-Fi to any robot or laptop using ROS in a seamless manner. The system is also versatile, as it can be directly used with practically any EMAT probe. Moreover, all the hardware of the system uses low power electronics of a maximum of 15 W. Experimental tests showed that the system has an SNR of 25 dB on steel and 15 dB on aluminum. The tests also showed that plate thickness could be measured to 0.1 mm accuracy on aluminum and steel plates. It was also shown that the system can work with different EMAT transducers, e.g. to excite and receive guided waves. This indicates that the system can be reliably used for inspections, although field tests are required to validate the system to use it in industry. These field tests in environments such as offshore are planned to be conducted in future work.

Acknowledgment

The authors would also like to thank Gabor Gubicza for his help in the development of the system electronics.

References

[1] A. Ollero *et al.*, "The AEROARMS project: Aerial robots with advanced manipulation capabilities for inspection and maintenance," *IEEE Robot. Automat. Mag.*, vol. 25, no. 4, pp. 12–23, Dec. 2018.

[2] M. Bengel, K. Pfeiffer, B. Graf, A. Bubeck, and A. Verl, "Mobile robots for offshore inspection and manipulation," in *Proc. IEEE/RSJ Int. Conf. Intell. Robots Syst.*, Oct. 2009, pp. 3317–3322.

[3] Y. T. Showcase, "Sensabot: A safe and cost-effective inspection solution," *J. Petroleum Technol.*, vol. 64, no. 10, pp. 32–34, Oct. 2012, doi: 10.2118/1012-0032-JPT.

[4] A. F. Moghaddam, M. Lange, O. Mirmotahari, and M. Hovin, "Novel Mobile Climbing Robot Agent for Offshore Platforms," *Int. J. Mech. Mechatronics Eng.*, vol. 6, no. 8, pp. 1353–1359, 2012.

[5] M. Hutter *et al.*, "ANYmal—A highly mobile and dynamic quadrupedal robot," in *Proc. IEEE/RSJ Int. Conf. Intell. Robots Syst. (IROS)*, Oct. 2016, pp. 38–44.

[6] L. L. Whitcomb, "Underwater robotics: Out of the research laboratory and into the field," in *Proc. ICRA Millennium Conf. IEEE Int. Conf. Robot. Automat. Symposia*, Apr. 2000, pp. 709–716.

[7] J. Elvander and G. Hawkes, "ROVs and AUVs in support of marine renewable technologies," in *Proc. Oceans*, Oct. 2012, pp. 1–6

[8] H. Hastie *et al.*, "The ORCA hub: Explainable offshore robotics through intelligent interfaces," in *Proc. 13th Annu. ACM/IEEE Int. Conf. Hum. Robot Interact., HRI Workshop Explainable Robot. Syst.*, Chicago, IL, USA, 2018, pp. 1–2. [Online]. Available: https://arxiv.org/pdf/1803.02100.pdf

[9] (2019). *Sprint Robotics*. [Online]. Available: www.sprintrobotics.org

[10] M. Hirao and H. Ogi, *Emats for Science and Industry: Noncontacting Ultrasonic Measurements*. Norwell, MA, USA: Kluwer, 2003.

[11] R. Ribichini, F. Cegla, P. B. Nagy, and P. Cawley, "Evaluation of electromagnetic acoustic transducer performance on steel materials," in *Proc. AIP Conf.*, 2011, vol. 1335, no. 1, pp. 785–792.

[12] J. Isla, M. Seher, R. Challis, and F. Cegla, "Optimal impedance on transmission of Lorentz force EMATs," in *Review of Progress in Quantitative Nondestructive Evaluation*. College Park, MD, USA: American Institute of Physics, 2016.

[13] M. Quigley *et al.*, "ROS: An open-source robot operating system," in *Proc. ICRA Workshop on Open Source Softw.*, May 2009, p. 5.

[14] J. Isla and F. Cegla, "EMAT phased array: A feasibility study of surface crack detection," *Ultrasonics*, vol. 78, pp. 1–9, Jul. 2017.

[15] P. Khalili and P. Cawley, "The choice of ultrasonic inspection method for the detection of corrosion at inaccessible locations," *NDT E Int.*, vol. 99, pp. 80–92, Oct. 2018.

Arnau Garriga-Casanovas received the D.Eng. degree from the Imperial College London in 2018, working in a collaborative project with Rolls-Royce plc., on the development of robots for *in situ* inspections. He is currently a Postdoctoral Researcher with the Imperial College, working on the use of robots for inspections as part of the ORCA Hub. During his EngD, he was awarded an industrial fellowship from the Royal Commission for the Exhibition of 1851.

Pouyan Khalili was born in Tehran, in 1991. He received the M.Eng. (Hons.) degree in mechanical engineering from the University College London (UCL), London, U.K., in 2014, the Ph.D. degree with the Non-Destructive Testing Group, Imperial College London, London, U.K., in 2018, focusing on high-frequency guided waves and other methods of corrosion monitoring applied in petrochemical plants. He is currently a Research Associate with the NDE Group, Imperial College London, where he is working as part of the ORCA Hub.

Frederic Cegla (Member, IEEE) is a Reader with the Non-Destructive Evaluation (NDE) Group, Mechanical Engineering Department, Imperial College London. His research interests are in the fields of NDE, structural health monitoring (SHM) and physical acoustics. He currently chairs the Physical Acoustics Group, Institute of Physics of the U.K. and Ireland. He has been the holder of a prestigious EPSRC Fellowship and has won numerous awards, such as the 2016 Achenbach Medal for his contribution to the field of SHM over the last decade. He has an interest and track record in protecting and commercializing technology, the biggest success so far being the formation of Permasense Ltd., a company that pioneered ultrasonic corrosion monitoring via autonomous wireless sensors.